https://doi.org/10.1016/j.compstruct.2020.112684

Behaviour of RC beams with a fibre-reinforced polymer (FRP)-strengthened web opening

X.F. Nie[1], S.S. Zhang[2, *] and T. Yu[3]

[1] Post-doctoral Fellow, School of Civil Engineering and Mechanics, Huazhong University of Science and Technology, Wuhan 430074, China.
[2] Professor, School of Civil Engineering and Mechanics, Huazhong University of Science and Technology, Wuhan 430074, China. (Corresponding author), E-mail address: shishun@hust.edu.cn
[3] Professor, Department of Civil and Environmental Engineering, The Hong Kong Polytechnic University, Hong Kong, China.

Abstract:

The beam opening (BO) technique, which involves (1) the creation of a web opening in the beam to weaken its flexural capacity and (2) the fibre-reinforced polymer (FRP) shear strengthening around the opening to avoid shear failure of the beam, was proposed to realize the strong column-weak beam hierarchy in existing reinforced concrete (RC) frames, which were designed using previous codes and thus violated such hierarchy. In the present study, six large-scale T-section beams with a web opening of different sizes and made by different methods (pre-formed and post-cut) were tested to assess the effectiveness of BO technique and the test results are presented. The experimental study show that the post-cutting method is feasible for making web openings in existing RC beams, the BO technique can effectively reduce the flexural capacity of the beam to the desired value if the size of web opening is appropriate, and the FRP strengthening can well compensate the loss of shear capacity and ductility of the beam caused by the creation of web opening. The present study provides a basis for the safe use of BO technique to achieve the strong column-weak beam hierarchy in existing RC frames.

Keywords: reinforced concrete (RC); beam opening; fibre-reinforced polymer (FRP) strengthening; strong column-weak beam; seismic performance

1. INTRODUCTION

For reinforced concrete (RC) frames subjected to seismic effects, there are mainly two possible failure modes: beam-sway mechanism (i.e., plastic hinges first form at the ends of beams) and story-sway mechanism (i.e., plastic hinges first form at the ends of columns). Beam failure usually affects only a limited part of the structure, while column failure may lead to progressive collapse of the whole structure. Therefore, beam-sway mechanism is preferred to story-sway mechanism if the failure of RC frames cannot be avoided. The strong column-weak beam design philosophy which can realize the beam-sway mechanism has been widely adopted in the seismic design of RC frames, according to a comprehensive literature review conducted by the authors [1]. To achieve the strong column-weak beam hierarchy in RC frames, a flexural strength ratio (i.e., ratio of the sum of flexural capacities of the columns at a joint to that of the beams framing into the joint) greater than 1 has been stipulated in the relevant design codes from different countries [1]. For instance, the current ACI code [2] and Eurocode [3] specify a flexural strength ratio of 1.2 and 1.3 respectively, and the current Chinese code [4] specifies a range of flexural strength ratio from 1.1 to 1.7.

However, studies have shown that the beam-sway mechanism rarely formed in failed RC frames after large earthquakes [e.g. 5-7], although these frames were designed to achieve the strong column-weak beam hierarchy. For example, after the magnitude (Ms) 8.0 Wenchuan earthquake in 2008, only RC frames without floor slabs or with precast floor slabs exhibited the beam-sway mechanism, while the cast-in-place RC frames commonly failed at the ends of columns [6]. This is mainly because that the contribution of cast-in-place slab to the flexural capacity of the beam was not properly considered in design codes of previous versions, leading to an underestimation of the flexural capacity of beam and thus the violation of the strong column-weak beam hierarchy. For instance, the Chinese seismic design code of previous versions [e.g. 8] ignored the contribution of cast-in-place floor slab to both the negative flexural capacity (i.e., the flange of the beam is in tension) and the positive flexural capacity (i.e., the flange of the beam is in compression) of the supporting beam [9]. Existing experimental studies on RC exterior/interior joints with a cast-in-place floor slab have confirmed that the floor slab can significantly enhance the flexural capacity of the beam, especially when the beam is in negative bending [e.g. 10-20]. Therefore, it is not unreasonable to believe that many existing RC frames in China and other countries/regions are likely to violate the strong column-weak beam requirement. The current design codes [e.g. 2-4] require the consideration of the contribution of the cast-in-place slabs to the flexural capacity of the beams. A larger number of existing RC frames, however, cannot meet this requirement and need to be retrofitted.

In order to achieve the strong column-weak beam hierarchy of an existing cast-in-place RC frame which violates such hierarchy, the strengthening of column is a straightforward option [e.g. 21-27]. There are mainly three common column strengthening techniques: (1) concrete jacketing [e.g. 21, 22]; (2) steel jacketing [e.g. 23, 24]; and (3) fibre-reinforced polymer (FRP) jacketing [e.g. 25-27]. However, concrete jacketing or steel jacketing results in the increase in seismic forces by increasing the mass and/or stiffness of the columns, while the FRP jacketing is not effective enough for non-circular columns, compared with that for circular columns [28]. Furthermore, the successful strengthening of column may simply shift the failure location from the column ends to the beam-column joint, which is more difficult to retrofit. Against the above background, a novel seismic retrofit method was proposed to achieve good seismic performance of cast-in-place RC frames which violate the strong column-weak beam requirement, based on the concept of Beam-end Weakening in combination with FRP Strengthening (referred to as BWFS method hereinafter for simplicity) [29]. Three specific techniques were proposed to implement the BWFS method [29]: (1) the beam opening (BO) technique; (2) the slab slit (SS) technique; and (3) the beam section reduction (SR) technique. More details of the above three techniques can be found in Ref. [29], and the present study is focused on the BO technique. The BO technique involves the creation of a web opening in the T-section beam adjacent to the beam-column joint and the installation of local shear strengthening system (e.g., using FRP wraps and FRP U-jackets) around the opening (as shown in Fig. 1). It should be noted that the strong column-weak beam design philosophy requires that the Sum of Flexural Capacities (referred to as SFC hereafter for simplicity) of the beam at a joint (i.e., the sum of positive and negative flexural capacities of the beam) are smaller than that of the column at the same joint. If the size of the web opening is suitable, the SFC of the T-section beam can be ideally reduced to a desired value (i.e., the SFC of the corresponding rectangular beam). Compared with other shapes of web openings such as circular and elliptical web openings, rectangular web opening can be more flexibly designed to achieve a required reduction of the flexural capacity of the T-section beam, and at the same time, rectangular web opening leads to regular shapes of the chords which can facilitate the development of design methods. Therefore, rectangular web opening is adopted in the BO technique. Meanwhile, to prevent the brittle shear failure of the beam with a web opening, the shear strengthening using FRP is applied around the opening. Actually, creating web openings in existing RC beams is not a new thing. It has been widely adopted in practice for the passages of utility pipes [e.g. 30-32].

A preliminary study has been conducted by the authors [33] to experimentally assess the concept of the BO technique in reducing the flexural capacity of the T-section beam. In the preliminary study [33], a total of eight RC beams, including one rectangular beam and seven T-section beams were tested. The rectangular beam (CB-Rec) and one T-section beam (CB-T) did not contain web openings and served as control specimens, while the remaining six T-section beams had a web opening. Two different web opening sizes (length × height being 700 mm × 300 mm and 800 mm × 280 mm respectively, referred to as web openings of large size) were examined. For each large web opening size, three beams were tested: one with an un-strengthened web opening (tested under negative bending) and two with an FRP-strengthened web opening (one tested under negative bending and the other one tested under positive bending).

In the preliminary study [33], the adopted web opening sizes were found to be too large so that the flexural capacity of the T-section beam was largely over-weakened. In addition, the web openings in the preliminary study [33] were pre-formed through manipulating the formwork for casting concrete, which is a simplification for test and not feasible for retrofitting of existing structures. The post-cut web opening, which is more practical for existing structures, needs to be investigated. To more comprehensively verify the effectiveness of the BO technique and to gain an improved and in-depth understanding on the behaviour of RC beams with a web opening, large-scale tests on RC beams with a pre-formed/post-cut web opening of more reasonable sizes were conducted and the test results are presented and analysed in the present study. In this paper, unless otherwise specified: (1) when presenting the test results, it is assumed that the web opening is located in the right shear span of the beam (i.e., the left opening edge refers to the edge closer to the loading point while the right opening edge refers to the edge closer to the right support); and (2) for the sake of brevity, the concrete chords in the beam flange and beam web are respectively referred to as flange chord and web chord.

2. EXPERIMENTAL PROGRAM

2.1 Specimen details

A total of six large-scale RC T-section beams were tested under three-point bending in the present study. The studied parameters included the web opening size (i.e., length × height) and the effect of FRP strengthening. Four different web opening sizes (length × height being 600 mm × 220 mm, 700 mm × 200 mm, 600 mm × 280 mm and 700 mm × 260 mm respectively) were investigated. For web openings of 600 mm × 220 mm and 700 mm × 200 mm (referred to as web openings of small size for simplicity), each web opening size contained two specimens with one having an un-strengthened web opening and the other one having an FRP-strengthened web opening. For web openings of 600 mm × 280 mm and 700 mm × 260 mm (referred to as web openings of medium size for simplicity), only specimens with an FRP-strengthened web opening were tested. The test specimens had the same dimensions: a total length of 3500 mm, a clear span of 3300 mm, a web thickness of 250 mm, an overall depth of 500 mm, a flange thickness of 100 mm and a flange width of 1450 mm. Details of the test specimens are listed in Table 1. Each specimen is given a name which consists of a letter to indicate whether FRP strengthening is applied (i.e., "O" for un-strengthened beam, and "F" for FRP-strengthened beam) and two three-digit numbers to show the length and height of the web opening respectively. It has been found from the preliminary study [33] that the behaviour of RC T-section beams with a web opening in positive bending is quite similar to that in negative bending. Moreover, the contribution of a cast-in-place floor slab to the flexural capacity of an RC beam in negative bending is much more significant than that in positive bending. Therefore, all specimens were tested in negative bending (i.e., the flange of the beam was in tension) in the present study.

The details of Specimen O-700×200 are plotted in Fig. 2 as an example to show the layout of the test specimens. As shown in Fig. 2, all specimens were such placed that they were all tested in negative bending. All six specimens had the same layout of longitudinal/shear steel reinforcement: three deformed steel bars of 20 mm in diameter were adopted as the primary compression reinforcement, four deformed steel bars of 20 mm in diameter were adopted as the primary tension reinforcement, and smooth steel bars of 8 mm in diameter with a spacing of 100 mm were adopted as the shear reinforcement; in addition, six smooth steel bars of 8 mm in diameter were adopted as the longitudinal reinforcement on each side of the beam flange (with three bars placed near the bottom surface while the other three bars near the top surface), and smooth steel bars of 8 mm in diameter with a spacing of 200 mm were adopted as the transverse reinforcement in the flange. The concrete cover was 30 mm within the beam web and 15 mm within the beam flange. The web opening was only created in the right shear span of the beam, and its location was determined as follows (Fig. 2): (1) the bottom edge of the web opening coincided with the web-flange intersection for ease of making the opening and subsequent theoretical studies; and (2) the horizontal distance between the left vertical edge of the web opening and the loading point was 250 mm, considering that the distance between the edge of the column and the nearer edge of the opening was assumed to be 250 mm, in order for the installation of the CFRP-U-jacket on the left side of the web opening (i.e., closer to the loading point).

2.2 Preparation of specimens

2.2.1 Formation of web opening

Two different approaches were adopted in the present study to make the web openings. In the first approach, through manipulating the formwork for casting the concrete, the web openings were pre-formed (i.e., the approach used in the preliminary study [33]). According to the size and location of the web opening, the stirrups intersected with the web opening were cut carefully. A typical pre-formed web opening is shown in Fig. 3. This approach is suitable for the new construction of RC beams with web openings but does not suit the scenario of web weakening of existing RC beams. Therefore, another approach was also examined in the present study to verify the feasibility of post-cutting web openings in the existing RC beams. In the second approach, the web openings were post-cut after 28 days' curing of the concrete by adopting the following four steps (as shown in Fig. 4): (1) drill small round holes along the boundary of the opening and cut the stirrups passing through the opening (Fig. 4a); (2) remove the concrete chunk to form a rough opening (Fig. 4b); (3) chip away the extrusive concrete by using an electric chisel along the boundary of the opening (Fig. 4c); and (4) polish the boundary of the opening by using a grinding machine (Fig. 4d). In the present study, the web openings in the three specimens with an opening length of 700 mm were prepared using the first approach and the rest three specimens with an opening length of 600 mm were prepared using the second approach, as shown in Table 1. Both approaches were proved to be feasible in fabricating the web opening.

2.2.2 Installation of FRP jackets

Carbon fibre-reinforced polymer (CFRP) was used for all four specimens with an FRP-strengthened web opening. The strengthening region is shown in Fig. 5a. After rounding the four corners of the web chord with a radius of 25 mm, one layer of CFRP sheet with a thickness of 0.334 mm was used to wrap the web chord. In addition, one layer of vertical CFRP U-jacket with a thickness of 0.334 mm and a width of 200 mm was adopted to strengthen the beam web at the two sides of the web opening (as shown in Fig. 5a), in order to prevent the development of possible diagonal cracks at the opening corners. The CFRP strengthening system was installed through wet-layup process and the detailed procedures were as follows: (1) use a needle gun to roughen the concrete surface (Fig. 6a); (2) use a clean brush to apply well-mixed primer (Sikadur 330) onto the concrete surface (Fig. 6b); (3) impregnate the carbon fibre sheets with well-mixed epoxy (Sikadur 300) and lay onto the concrete surface (Fig. 6c); and (4) evenly distribute the resin and release air bubbles through slowly rolling the FRP sheet (Fig. 6d).

2.2.3 Fabrication and installation of CFRP spike anchors

CFRP spike anchors which were made from the same type of carbon fibres used in the CFRP wraps and U-jackets were adopted to anchor the ends of the CFRP U-jackets to the beam flange (as shown in Fig. 5), in order to prevent the CFRP U-jackets from premature debonding. As can be seen from Figs. 5b and c, the CFRP spike anchors consist of two parts: anchor dowel and anchor fan. The anchor dowel is a hardened bundle of carbon fibres with a length of 90 mm and a diameter of around 11 mm. The anchor fan is a loose fibre tail with a length of 80 mm. The installation of CFRP spike anchors included two steps: (1) insert the anchor dowel into the predrilled holes filled with epoxy in the beam flange (the holes were evenly distributed along the web-flange intersection at a distance of 50 mm and drilled towards the direction of the mid-width of the cross section, and the inclination angle between the holes and the side surface of the beam web was 20 degrees, as shown in Figs. 5a and b); and (2) bond the anchor fan onto the ends of the CFRP U-jackets during the wet-layup process. As shown in Fig. 5a, four CFRP spike anchors which were evenly distributed with a spacing of 50 mm were used for each end of the CFRP U-jackets.

2.3 Material properties

In the present study, commercial concrete of normal strength was used. On the same day of beam test, three concrete cylinders (150 mm × 300 mm) were tested for each beam specimen to obtain the cylinder compressive strength of concrete. The average concrete strength of each beam specimen is shown in Table 1.

The material properties of steel bars used in this study were determined through standard tensile tests according to BS-18 [34]. The yield stress and ultimate stress of the deformed steel bars of 20 mm in diameter were 434 MPa and 559 MPa respectively, and the yield stress and ultimate stress of the smooth steel bars of 8 mm in diameter were 349 MPa and 526 MPa respectively. The elastic moduli of the steel bars of 20 mm in diameter and 8 mm in diameter were measured to be 203 GPa and 196 GPa, respectively.

Following ASTM D3039 [35], the material properties of CFRP sheet were determined through tensile tests on 7 coupons. The length and width of the test region of the CFRP coupons were 250 mm and 25 mm respectively. According to the nominal thickness of the CFRP sheet (0.334 mm per ply), its tensile strength and elastic modulus were measured to be 2820 MPa and 227 GPa respectively.

2.4 Test set-up and instrumentation

In the present study, a total of 13 linear variable displacement transducers (LVDTs) were used to measure the deflections of each beam specimen, with the layout of the LVDTs shown in Fig. 7. Six LVDTs were installed on the bottom surface of the beam flange, with three LVDTs (one was installed at the mid-width of the beam flange and the other two were respectively installed 300 mm away from the nearer edge of the beam flange) installed at the mid-span of the beam (i.e., 01, 02 and 03 shown in Fig. 7) and the mid-span of the web opening (i.e., 04, 05 and 06 shown in Fig. 7), respectively. Two LVDTs were installed on the top surface of the beam web at the two supports (i.e., 07 and 08 shown in Fig. 7). The rest five LVDTs were evenly distributed on the top surface of the web chord (i.e., 09 to 13 shown in Fig. 7).

In addition, a large number of strain gauges were used to measure the strain development of the steel bars and FRP. The strain gauge arrangement of the steel bars in all test specimens was all the same. Taking Specimen F-700×200 as an example, the layout of strain gauges on the steel bars is shown in Fig. 8. As can be seen from Fig. 8a, the whole longitudinal steel bars were divided into three groups: top steel bars, middle steel bars and bottom steel bars. The top steel bars included the three bars in the compression zone; the middle steel bars included the six bars in the beam flange nearer the top surface of the flange; and the bottom steel bars included the ten bars nearer the bottom surface of the beam flange (i.e., four bars in the web and six in the flange). For the top steel bars, strain gauges were installed onto two bars including the middle one (Fig. 8b); for each selected bar, the strains of the following four critical positions were monitored using strain gauges: positions corresponding to the mid-span of the beam, the mid-span and the two vertical edges of the web opening, respectively. For the bottom steel bars, strain gauges were installed onto a half of the bars in the same side of the beam (i.e., two bars in the web and three in the flange, taking advantage of symmetry) and the outmost bar in the other side of the beam (Fig. 8c); the arrangement of the strain gauges for all selected bottom steel bars were the same as that for the top steel bars. For the middle steel bars, strain gauges was installed onto the two middle bars in each side of the flange (Fig. 8d); for each selected bar, only the strain of the position corresponding to the mid-span of the beam was monitored using one strain gauge.

Fig. 9 shows the layout of strain gauges on the CFRP strengthening system for specimens with an FRP-strengthened web opening. For the two CFRP U-jackets, only the strains of one arm of the jackets were monitored using strain gauges by taking advantage of symmetry; a total of eight strain gauges were used, with four evenly distributed strain gauges vertically attached on each CFRP U-jacket (i.e., along the fibre direction of the CFRP). For the CFRP wrap on the web chord, the strains of three critical positions (i.e., the mid-span and the two ends of the web chord) were monitored using a total of 15 strain gauges, with five strain gauges on each critical position (two on the bottom surface of the chord, one on the side surface of the chord and two on the top surface of the chord), as shown in Fig. 9. The strain gauge on the side surface of the chord was applied at the mid-height of the chord and in the hoop direction of the CFRP wrap; one of the two strain gauges on the top/bottom surface of the chord was applied at the mid-width of the chord and in the hoop direction of the CFRP wrap, and the other one was also applied at the mid-width of the chord but in the longitudinal direction of the web chord.

All six beam specimens were tested under three-point negative bending with the test set-up shown in Fig. 10. The load was applied at the mid-span of the beam through a hydraulic jack.

3. TEST RESULTS

3.1 Failure mode

The failure modes of all test specimens are shown in Fig. 11. For the two specimens with an un-strengthened web opening of small size (i.e., O-600×220 and O-700×200), the first crack appeared at the top-left corner of the web opening (i.e., the opening corner nearest to the loading point) and extended diagonally towards the loading point (around 45 degrees with respect to the horizontal direction). Then a horizontal crack between the flange and the web appeared at the bottom-right corner of the web opening (i.e., the opening corner nearest to the right support). Afterwards, diagonal cracks (around 30 to 45 degrees with respect to the horizontal direction) occurred and further developed in the web chord, which finally dominated the failure of the specimens (Figs. 11a and b). It should be noted that the failure modes of specimens with an un-strengthened web opening of small size tested in the present study are quite different from the failure modes of specimens with an un-strengthened web opening of large size tested in the preliminary study (i.e., O-700×300 and O-800×280) [33], which were controlled by the combined local mixed flexural and shear actions at the right end of the flange chord as well as the left end of the web chord, and the local flexural failure (i.e., crushing of concrete in compression) at the left end of the flange end as well as the right end of the web chord.

For the four specimens with an CFRP-strengthened web opening (two with a web opening of small size and two with a web opening of medium size), the existence of the CFRP wraps and CFRP U-jackets well prevented/mitigated the initiation/development of shear cracks in the web chord and the corners of the web opening. As can be seen from Figs. 11c-f, due to the presence of the web opening, the left ends of the flange and web chords were under a sagging moment while the right ends of the flange and web chords were under a hogging moment, which is quite different from the behaviour of RC T-section beams without a web opening. The final failure of all these four specimens was dominated by the flexural failure at the two ends of the flange chord as well as the web chord, with plastic hinges formed clearly at the two ends of the flange and web chords (Figs. 11c-f), which was similar to the failure modes of specimens with an FRP-strengthened web opening tested in the preliminary study [33].

3.2 Load-deflection response of the beam

Load-deflection curves of the test specimens are shown in Fig. 12, in which the horizontal axis shows the mid-span deflection, averaged from the readings of the three LVDTs 01, 02 and 03 shown in Fig. 7. The key results (including cracking load, yield load and ultimate load which is the maximum recorded load) are listed in Table 2. In the present study, numerical results of the control beams (i.e., rectangular and T-section beams without a web opening) obtained from finite element (FE) modelling were used for the comparisons of the test results. In the FE modelling, the concrete was modelled using the concrete damaged plasticity model available in ABAQUS [36], and the bond behaviour between concrete and internal steel reinforcements was properly considered. The accuracy of this FE model has been verified with the test results in the preliminary study [33]. The predicted load-deflection curves and key results (cracking load and yield load) of the two control beams (referred to as CB-Rec-2 for rectangular control beam and CB-T-2 for T-section control beam respectively) obtained from the FE modelling are respectively shown in Fig. 12 and Table 2 for references. As can be seen from Fig. 12, due to the existence of a flange (i.e., cast-in-place floor slab in a real structure), Specimen CB-T-2 has much larger flexural capacity and stiffness than Specimen CB-Rec-2, indicating that the flange can significantly enhance the flexural capacity and stiffness of the beam in negative bending. Moreover, it should be noted that for all test specimens in this study, the yield strain of the bottom steel bars at the mid-span of the beam was not reached during the loading process. As a result, the yield load F_y for the control specimens (as listed in Table 2) cannot be obtained for RC beams with a web opening. Instead, the load corresponding to yielding of the bottom steel bars at the left end of the flange chord (F_{y1}) and the load corresponding to yielding of the steel bars at the right end of the web chord (F_{y2}) were obtained and listed in Table 2.

3.2.1 Specimens with a web opening of small size

The load-deflection curves of Specimens O-600×220 and O-700×200 having an un-strengthened web opening of small size are shown in Fig. 12a. The initial stiffness of Specimens O-600×220 and O-700×200 was similar to that of Specimen CB-Rec-2. After cracking of concrete, their stiffness decreased and was a little lower than that of CB-Rec-2. Shortly after yielding of the specimen, the load experienced an abrupt drop (around 30%-35% of the yield load) due to the brittle shear failure in the web chord and then gradually dropped to around half of the yield load. As shown in Table 2, the cracking loads of Specimens O-600×220 and O-700×200 were respectively around 160 % and 120% of that of Specimen

CB-Rec-2, the yield loads were respectively around 74% and 79% of that of Specimen CB-Rec-2, and the ultimate loads were respectively around 99% and 94% of that of Specimen CB-Rec-2.

With FRP strengthening (i.e., Specimens F-600×220 and F-700×200), the load did not experience a sudden drop after yielding of the specimens, revealing a significantly improved ductility of the specimens, as shown in Fig. 12a. As can be seen from Table 2, the cracking loads of Specimens F-600×220 and F-700×200 were both around 202% of the Specimen CB-Rec-2, the yielding loads were both around 89% of that of Specimen CB-Rec-2, and the ultimate loads were respectively around 121% and 128% of that of Specimen CB-Rec-2.

3.2.2 Specimens with a web opening of medium size

To further investigate the effect of web opening size on the behaviour of RC T-section beams, two specimens with an FRP-strengthened web opening of medium size (i.e., Specimens F-600×280 and F-700×260) were tested. It can be seen from Fig. 12b that the shapes of the load-deflection curves of Specimens F-600×280 and F-700×260 are quite similar to those of the two control specimens (i.e., CB-Rec-2 and CB-T-2). As shown in Table 2, the cracking loads of the two specimens were both 76 kN which were around 152% of that of Specimen CB-Rec-2, and the ultimate loads were respectively around 81% and 84% of that of Specimen CB-Rec-2.

3.3 Deflection response of the web chord

The vertical deflections of the web chord were measured using five evenly distributed LVDTs along the span of the web chord (i.e., LVDTs 09-13 in Fig. 7). The deflections of the web chords of the test specimens are plotted in Fig. 13. As can be seen from Fig. 13, for all the selected load levels, the distributions of deflections along the span of the web chord are nearly linear. As the failure was postponed by the FRP strengthening system, specimens with an FRP-strengthened web opening have a larger ultimate deflection than the corresponding specimens with an un-strengthened web opening. Moreover, it is interesting to notice that the specimens with a web opening of small size (i.e., Specimens O-700×200, F-700×200, O-600×220 and F-600×220) only have downward defections (i.e., negative values in the figures) of the web chord over its span, while in the deflected shapes of the web chord of the specimens with a web opening of medium size (i.e., Specimens F-700×260 and F-600×280), a zero-deflection point (where the deflection is equal to zero) can be found, with the deflections being upward (i.e., positive values in the figures) on the right part of the web chord (i.e., closer to the right support) while downward on the left part (i.e., closer to the loading point). Combining the test results of the preliminary study [33], a further investigation of these deflected shapes indicates that a larger length-to-height ratio of the web chord gives a higher possibility of the formation of zero-deflection point in the span of the web chord. Furthermore, the relative position of the zero-deflection point is also dependent on the length-to-height ratio of the web chord: a larger ratio gives a larger relative distance from the zero-deflection point to the right end of the web chord (defined as the distance from the zero-deflection point to the right end of the web chord divided by the total length of the web chord). This is because a larger length-to-height ratio of the web chord leads to a smaller stiffness of the web chord and thus a larger upward deflection of the right end of the web chord under hogging bending. For example, the relative distance from the zero-deflection point to the right end of the web chord of Specimen F-800×280 is 0.25 (i.e., 200 mm/800 mm) [33], which is larger than that of Specimen F-600×280 (i.e., 0.17 =100 mm/600 mm). This is because the former specimen has a length-to-height ratio of the web chord of 6.7 (i.e., 800 mm/120 mm), which is larger than that of the latter specimen (i.e., 5.0 = 600 mm/120 mm).

3.4 Strains in the steel bars and FRP

An examination of the readings of strain gauges on steel bars and FRP showed that the general feature of strain distribution and development is similar for all specimens tested in the present study. The strain distributions in the steel bars revealed that the left ends of the flange and web chords were under a sagging moment (i.e., the bottom surface of the chord was in tension and the top surface of the chord was in compression), while the right ends of the flange and web chords were under a hogging moment (i.e., the bottom surface of the chord was in compression and the top surface of the chord was in tension). For all test specimens in the present study, the bottom steel bars at the left end of the flange chord (i.e., the positions where strain gauges B21-B26 in Fig. 8c installed) and the top steel bars at the right end of the web chord (i.e., the positions where strain gauges T41 and T42 in Fig. 8b installed) were all in tension and yielded during the loading process, while the steel bars at the other monitored positions (including the bottom steel bars at mid-span of the beam) did not yield, indicating that the failure of the beam was controlled by the failure of the chords.

The readings of the six longitudinal strain gauges on the FRP wrap (strain gauges WL1, WL2, WM1, WM2, WR1 and WR2 in Fig. 9) also showed that the bottom surface of the web chord at its left end (i.e., the position where strain gauge WL1 installed) and the top surface of the web chord at its right end (i.e., the position where strain gauge WR2 installed) were in tension, while the top surface of the web chord at its left end (i.e., the position where strain gauge WL2 installed) and the bottom surface of the web chord at its right end (i.e., the position where strain gauge WR1 installed) were in compression. Consequently, the hoop strains of the FRP wrap on top-left end of the web chord (i.e., the position where strain gauge WL5 in Fig. 9 installed) and the FRP wrap on bottom-right end of the web chord (i.e., the position where strain gauge WR3 in Fig. 9 installed) were both positive (i.e., the FRP was in tension), which was caused by the expansion of concrete due to the large compressive strain at these two positions. The readings of strain gauges WR3 and WL5 were both large [especially WR3, whose reading reached around 8000 $\mu\varepsilon$, exceeding half of the ultimate strain of the used CFRP (around 12800$\mu\varepsilon$)], indicating that the compressive concrete at the two ends of the web chord where plastic hinges formed was effectively confined by the FRP wrap.

4. EFFECT OF WEB OPENING SIZE

From the above comparisons, it can be seen that a larger web opening unsurprisingly gives a lower load-carrying capacity and stiffness of the RC T-section beam. It can be found from Fig. 12 and Table 2 that the reduction in the load-carrying capacity of the RC T-section beam caused by an increase of 100 mm in the web opening length is comparable to that caused by an increase of 20 mm in the web opening height (e.g., O-600×220 and O-700×200;

F-600×280 and F-700×260), which indicates that increasing the web opening height is more efficient than increasing the web opening length in reducing the load-carrying capacity of the RC T-section beam. Considering that the web opening height directly affects the height of the web chord, it can be reasonably deduced that the reduction in the load-carrying capacity of the RC T-section beam highly depends on the height of the web chord.

Moreover, the web opening size also affects the failure mode of the RC T-section beam. The RC T-section beams with an un-strengthened web opening of small size tested in the present study (i.e., O-600×220 and O-700×200) failed in a shear mode due to the formation of diagonal cracks in the web chord, while the failure of the RC T-section beams with an un-strengthened web opening of large size tested in the preliminary study (i.e., O-700×300 and O-800×280) [33] were controlled by the local flexural failure or the local mixed failure (flexural and shear) at the two ends of the web and flange chords. The web opening size directly influences the size of the web chord, and therefore influences the flexural and shear capacities of the web chord. It can be reasonably inferred that if the shear capacity of the web chord is smaller than its flexural capacity, shear failure will occur in the web chord (e.g., Specimens O-600×220 and O-700×200); while if the shear capacity of the web chord is larger than its flexural capacity, flexural failure will occur at the two ends of the web chord (e.g., Specimens F-600×220 and F-700×200). More studies, however, are needed to justify the above hypothesis.

5. EFFECT OF FRP STRENGTHENING

As can be seen from Figs. 11a-d, the existence of the FRP strengthening system which included CFRP U-jackets on the beam web with their ends anchored with the beam flange using spike anchors and CFRP wrap on the web chord contributed to changing the failure mode of the web opening-weakened RC T-section beam from shear failure in the web chord to flexural failure at the two ends of the web and flange chords. Moreover, it can be found from Fig. 12 that the adopted FRP strengthening system not only increased the stiffness and load-carrying capacity of the beam, but also enhanced the ductility of the beam significantly.

The performance enhancement of the RC T-section beam with a web opening due to the existence of the FRP strengthening system can be attributed to the following three reasons: (1) the CFRP wrap on the web chord can provide shear contribution to the web chord and thus enhance the load-carrying capacity of the beam; (2) the FRP U-jackets with spike anchors can restrict/mitigate the initiation/development of diagonal cracks at the opening corners and the horizontal cracks between the flange and the web, and therefore avoid the brittle behaviour of the beam caused by such cracks; and (3) the concrete in the web chord is effectively confined by the CFRP wrap and thus the compressive strength and ductility of the web chord can be enhanced significantly.

6. ASSESSMENT OF THE EFFECTIVENESS OF BO TECHNIQUE

As has been mentioned earlier, the proposed BO technique aims to reduce the SFC of the T-section beam to the desired value (i.e., the SFC of the corresponding rectangular beam). A strength model for RC beams with an FRP-strengthened web opening has been proposed by the author [37] based on the test results of the preliminary study [33]. In this section, the comparison of the strength of RC beams with an FRP-strengthened web opening between the prediction of the proposed model and the test results of present study will be made first to examine the accuracy of the proposed model. After further verification with the test results, the proposed model will be adopted to predict the positive flexural capacities of the specimens tested in this study and the effectiveness of the BO technique will be assessed through the comparison of SFCs of the beams.

6.1 Comparison of beam strength between prediction and test

In proposing the strength model [37], the top and the bottom chords which dominate the strength of RC beam with a web opening were isolated to form a free-body diagram (as shown in Fig. 14), based on which a series of force equilibrium equations can be set up. Through cross-sectional analyses, the simplified interaction diagrams between axial force (N) and bending moment (M) (referred to as N-M curves for simplicity) of the cross-sections at the two ends of the top and the bottom chords can be obtained, as shown in Fig. 15, in which the equations of the four *N*-*M* curves are given. It should be noted that, if the top/bottom chord is wrapped using FRP, the confinement effect from FRP to concrete should be properly considered when calculating the *N*-*M* curves. The reader can refer to Ref. [37] for more details. Combining the equations of the *N*-*M* curves with the force equilibrium equations, the ultimate of the beam can be figured out, as expressed in Eq. (1).

$$F = \frac{L}{L_{LS}} \frac{(b_{tL} + b_{bL})(z - a_{tR} - a_{bR}) + (b_{tR} + b_{bR})(z + a_{tL} + a_{bL})}{(z - a_{tR} - a_{bR})(L_R + l) - (z + a_{tL} + a_{bL})L_R} \tag{1}$$

where L is the clear span of the whole beam; L_{LS} is the left shear span of the beam; z is the distance between the midlines of the top and the bottom chords; L_R is the distance between the right end of the opening and the right support; l is the opening length; a_{tR}, b_{tR}, a_{tL}, b_{tL}, a_{bR}, b_{bR}, a_{bL} and b_{bL} are the coefficients of equations of the four *N*-*M* curves as shown in Fig. 15. For more details, the reader can refer to Ref. [37].

The predicted ultimate loads of the four RC T-section beams with an FRP-strengthened web opening are compared with test results in Table 3. It can be seen from Table 3 that the strength model gives very close predictions to the test results, with an average prediction-to-test ratio of 0.952, a standard deviation (STD) of 0.00778, and a coefficient of variation (CoV) of 0.00817.

6.2 Comparison of SFCs

The SFCs of the two control specimens (i.e., CB-Rec-2 and CB-T-2) as well as the four T-section beams with an FRP-strengthened web opening of small/medium size (600 mm × 220 mm, 700 mm × 200 mm, 600 mm × 280 mm and 700 mm × 260 mm) are listed in Table 4. It should be noted that the negative and positive flexural capacities of the two control specimens were obtained from the FE analyses, as has been explained earlier; the negative flexural capacities of the four T-section beams with an FRP-strengthened web opening were obtained from the tests; and the positive flexural capacities of the four T-section beams with an FRP-strengthened web opening were obtained from the strength model.

As can be seen from Table 4, the SFC of Specimen CB-T-2 is 146% of that of the rectangular control beam CB-Rec-2, which indicates that the flange (i.e., the existence of a floor slab in a real structure) has a substantial effect on the SFC of the beam. With the presence of an FRP-strengthened web opening of medium size (600 mm × 280 mm or 700 mm × 260 mm), the SFC of the T-section beam can be reduced to around 86% of that of the control beam CB-Rec-2; while with the presence of an FRP-strengthened web opening of small size (600 mm × 220 mm or 700 mm × 200 mm), the SFC of the T-section beam can be reduced to around 112% of that of the control beam CB-Rec-2. All these results indicate that the proposed BO technique is very effective in reducing the SFC of the T-section beam, and a web opening between the medium size and small size examined in this experimental study will be able to reduce the SFC of the T-section beam to the ideally desired value (i.e., the SFC of the corresponding rectangular beam). Moreover, the adopted FRP strengthening system in the present study including CFRP complete wrap on the web chord and CFRP U-jackets with spike anchors on the beam web can effectively prevent the web opening-weakened beam from failing in a brittle shear model, and significantly enhance the ductility of the beam. Therefore, this FRP strengthening system is necessary for the strengthening of web opening-weakened beams in practice.

7. CONCLUDING REMARKS

As the contribution of cast-in-place floor slabs to the flexural capacities of RC beams was not properly considered in the design based on previous codes, a large number of existing RC frames may violate the strong column-weak beam hierarchy. Based on the concept of Beam-end Weakening in combination with FRP Strengthening (BWFS) method, a novel seismic retrofit technique (BO technique) which involves the creation of a web opening in the T-section beam and the installation of FRP strengthening system around the opening was proposed. This paper first presents an experimental study on six large-scale RC T-section beams with a web opening of small/medium size to access the effectiveness of the BO technique in reducing the flexural capacity of the beam, then verifies the accuracy of the existing strength model for such FRP-strengthened RC beams with the test results, and finally compares the SFCs between T-section beams and rectangular beams. Based on the experimental and theoretical studies, the following conclusions can be drawn:

1) The proposed BO technique can effectively reduce the SFC of the RC T-section beam and making a web opening in an existing RC beam (i.e., post-cut opening) was proved to be feasible. Therefore, the BO technique can be an effective approach to achieve the strong column-weak beam hierarchy in existing RC frames which originally violate such hierarchy;
2) A larger web opening usually leads to a larger reduction of SFC of the beam, and increasing the height of web opening was found to be more efficient in reducing the SFC of the beam than increasing the length of web opening. The comparison of SFCs of the test beams revealed that for beams in the present study, a web opening between the medium size and small size will be able to reduce the SFC of the T-section beam to the desired value (i.e., the SFC of the corresponding rectangular beam). The size of the web opening, which is required to perfectly reduce the SFC of the T-section beam to the desired value, can be designed using the proposed strength model through a trial and error progress;
3) The proposed FRP strengthening system, including CFRP U-jackets with spike anchors on the beam web and CFRP wrap on the web chord, is necessary for the BO technique, as it can not only increase the shear capacity and stiffness of the beam but also significantly enhance the ductility of the beam; and
4) The accuracy of the strength model proposed by the authors was further verified with the test results of RC beams with an FRP-strengthened web opening of medium/small sizes in the present study, indicating that the strength model can be used for the prediction of flexural capacity of such FRP-strengthened beams.

ACKNOWLEDGEMENTS

The authors are grateful for the financial support received from the Research Grants Council of the Hong Kong Special Administrative Region (Project No.: PolyU 5273/11E) and the

National Natural Science Foundation of China (Project No. 51878310). The work presented in this paper was undertaken under the supervision of Prof. Jin-Guang Teng from The Hong Kong Polytechnic University. The authors are grateful to Prof. Teng for his contributions to this work.

DATA AVAILABILITY

The raw/processed data required to reproduce these findings cannot be shared at this time as the data also forms part of an ongoing study.

REFERENCES

[1] Nie, X.F., Zhang, S.S., Jiang, T. and Yu, T. (2020). "The strong column-weak beam design philosophy in reinforced concrete frame structures: A literature review", *Advances in Structural Engineering*, accepted.

[2] ACI-318 (2019). *Building code requirements for structural concrete and commentary (ACI 318-19)*, ACI Committee 318, American Concrete Institute, Farmington Hills, MI.

[3] Eurocode-8 (2004). *Design of structures for earthquake resistance – part 1: general rules, seismic actions and rules for buildings (EN 1998-1: 2004)*, CEN, Brussels.

[4] GB-50011 (2010). *Code for seismic design of buildings*, Architectural & Building Press, Beijing, China (in Chinese).

[5] ATC-40 (1996). *Seismic evaluation and retrofit of concrete buildings*, Applied Technology Council, Redwood City, California.

[6] Chinese Academy of Building Research (CABR) (2008). *Photo collection of 2008 Wenchuan Earthquake damage to buildings*, China Architectural & Building Press, Beijing, China (in Chinese).

[7] Chen, H., Xie, Q.C., Dai, B.Y., Zhang, H.Y. and Chen, H.F. (2016). "Seismic damage to structures in the Ms 6.5 Ludian earthquake", *Earthquake Engineering and Engineering Vibration*, 15(1), 173-186.

[8] GB-50011 (2008). *Code for seismic design of buildings*, Architectural & Building Press, Beijing, China (in Chinese).

[9] Lin, X., Pan, P., Ye, L., Lu, X. and Zhao, S. (2009). "Analysis of the damage mechanism of a typical RC frame in Wenchuan earthquake", *China Civil Engineering Journal*, 42(5), 13-20 (in Chinese).

[10] Ehsani, M.R. and Wight, J.K. (1985). "Effect of transverse beams and slab on behavior of reinforced concrete beam to column connections", *ACI Journal*, 82(2), 188-195.

[11] Durrani, A.J. and Wight, J.K. (1987). "Earthquake resistance of reinforced concrete interior connections including a floor slab", *ACI Journal*, 84(5), 400-406.

[12] Pantazopoulou, S.J. and Moehle, J.P. (1990). "Identification of effect of slabs on flexural behavior of beams", *Journal of Engineering Mechanics*, ASCE, 116(1), 91-106.

[13] Zerbe, H.E. and Durrani, A.J. (1990). "Seismic response of connections in two-bay reinforced concrete frame subassemblies with a floor slab", *ACI Structural Journal*, 87(4), 406-415.

[14] Guimaraes, G.N., Kreger, M.E. and Jirsa, J.O. (1992). "Evaluation of joint-shear provisions for interior beam-column-slab connections using high-strength materials", *ACI Structural Journal*, 89(1), 89-98.

[15] Siao, W.B. (1994). "Reinforced concrete column strength at beam/slab and column intersection", *ACI Structural Journal*, 91(1), 3-8.

[16] LaFave, J.M. and Wight, J.K. (1999). "Reinforced concrete exterior wide beam-column-slab connections subjected to lateral earthquake loading", *ACI Structural Journal*, 96(4), 577-587.

[17] Pantazopoulou, S.J. and French, C.W. (2001). "Slab participation in practical earthquake design of reinforced concrete frames", *ACI Structural Journal*, 98(4), 479-489.

[18] Shin, M. and LaFave, J.M. (2004). "Seismic performance of reinforced concrete eccentric beam-column connections with floor slabs", *ACI Structural Journal*, 101(3), 403-412.

[19] Shin, M. and LaFave, J.M. (2004). "Reinforced concrete edge beam-column-slab connections subjected to earthquake loading", *Magazine of Concrete Research*, 55(6), 273-291.

[20] Canbolat, B.B. and Wight, J.K. (2008). "Experimental investigation on seismic behavior of eccentric reinforced concrete beam-column-slab connections", *ACI Structural Journal*,

105(2), 154-162.

[21] Thermou, G.E., Pantazopoulou, S.J. and Einashai, A.S. (2007). "Flexural behavior of brittle RC members rehabilitated with concrete jacketing", *Journal of Structural Engineering*, ASCE, 133(10), 1373-1384.

[22] Campione, G., Fossetti, M., Giacchino, C. and G. Minafò. (2014). "RC columns externally strengthened with RC jackets", *Materials and Structures*, 47(10), 1715-1728.

[23] Xiao, Y. and Wu, H. (2003). "Retrofit of reinforced concrete columns using partially stiffened steel jackets", *Journal of Structural Engineering*, ASCE, 129(6), 725-732.

[24] He, A., Cai, J., Chen, Q.J., Liu, X., Xue, H. and Yu, C. (2017). "Axial compressive behaviour of steel-jacket retrofitted RC columns with recycled aggregate concrete", *Construction and Building Materials*, 141, 501-516.

[25] Teng, J.G., Chen, J.F., Smith, S.T. and Lam, L. (2002). *FRP-strengthened RC structures*, John Wiley and Sons Ltd, UK, November, 245pp.

[26] Hadi, M.N.S. (2007). "Behaviour of FRP strengthened concrete columns under eccentric compression loading", *Composite Structures*, 77(1), 92-96.

[27] Teng, J.G., Lam, L., Lin, G., Lu, J.Y. and Xiao, Q.G. (2016). "Numerical simulation of FRP-jacketed RC columns subjected to cyclic and seismic loading", *Journal of Composites for Construction*, ASCE, 20(1), 04015021.

[28] Lam, L. and Teng, J.G. (2003). "Design-oriented stress-strain model for FRP-confined concrete in rectangular columns", *Journal of Reinforced Plastics and Composites*, 22(13), 1149-1186.

[29] Teng, J.G., Zhang, S.S., Jing, D.H., Nie, X.F. and Chen, G.M. (2013). "Seismic retrofit of RC frames through beam-end weakening in conjunction with FRP strengthening", *Proceedings of the 4th Asia-Pacific Conference on FRP in Structures (APFIS 2013)*, 1-8.

[30] Mansur, M.A., Tan K.H. and Wei, W. (1999). "Effects of creating an opening in existing beams", *ACI Structural Journal*, 96(6), 899-906.

[31] Maaddawy, T. and Sherif, S. (2009). "FRP composite for shear strengthening of reinforced concrete deep beams with openings", *Composite Structures*, 89(1), 60-69.

[32] Maaddawy, T. and El-Ariss, B. (2012). "Behavior of concrete beams with short shear span and web opening strengthened in shear with CFRP composites", *Journal of Composites for*

Construction, ASCE, 16(1), 47-59.

[33] Nie, X.F., Zhang, S.S., Teng, J.G. and Chen, G.M. (2018). “Experimental study on RC T-section beams with an FRP-strengthened web opening”, *Composite Structures*, 185, 273-285.

[34] BS-18 (1987). *Method for tensile testing of metals*, British Standards Institution, London, U.K.

[35] ASTM D3039 (2014). *Standard test method for tensile properties of polymer matrix composite materials*, ASTM International, West Conshohocken, PA.

[36] ABAQUS (2012). *ABAQUS Analysis User's Manual (Version 6.12)*, Dassault Systems SIMULIA Corporation, Providence, Rhode Island, USA.

[37] Nie, X.F. and Zhang, S.S. (2020). “Strength model for RC beams with an FRP-strengthened web opening”, submitted to *Composite Structures*.

Table 1. Specimen details

Specimen	Opening size		Web/flange chord height (mm)	FRP strengthening	Bending direction	Fabrication of web opening	Cylinder compressive strength of concrete f_c (MPa)
	Length (mm)	Height (mm)					
O-600×220	600	220	180/100	No	Negative bending[(a)]	Post-cut	40.3
F-600×220				Yes	Negative bending	Post-cut	40.3
O-700×200	700	200	200/100	No	Negative bending	Pre-formed	36.2
F-700×200				Yes	Negative bending	Pre-formed	39.6
F-600×280	600	280	120/100	Yes	Negative bending	Post-cut	42.0
F-700×260	700	260	140/100	Yes	Negative bending	Pre-formed	42.0

Note: (a) The beam flange was in tension.

Table 2. Key results

Specimen	Cracking load F_{cr} (kN)	Yield load F_y (kN)	Yield load F_{y1} [(a)] (kN)	Yield load F_{y2} [(b)] (kN)	Ultimate load F_u (kN)	Cracking load ratio[(c)] (%)	Ratio of yield load F_{y1} [(c)] (%)	Ultimate load ratio[(c)] (%)	Gain in flexural capacity due to CFRP (%)
CB-Rec-2 (FE)	50	320			320				
CB-T-2 (FE)	146	500			500				
O-600×220	80		238	316	316	160.0	74.4	98.8	
F-600×220	101		284	NA[(d)]	388	202.0	88.8	121.3	24.0
O-700×200	60		253	291	300	120.0	79.1	93.8	
F-700×200	101		284	NA[(d)]	410	202.0	88.8	128.1	31.3
F-600×280	76		NA[(d)]	211	260	152.0	NA[(d)]	81.3	
F-700×260	76		196	199	270	152.0	61.3	84.4	

Note:
(a) F_{y1}= load at yielding of the bottom steel bars at the left end of flange chord;
(b) F_{y2}= load at yielding of the top steel bars at the right end of web chord;
(c) Ratio between web opening-weakened T-section beam and rectangular control beam;
(d) The relevant strain gauge was damaged during loading.

Table 3. Verification of the proposed strength model [35]

Specimen	Test (kN)	Prediction (kN)	Prediction / Test
F-600×280	256	246	0.961
F-700×260	265	252	0.951
F-600×220	380	358	0.942
F-700×200	388	370	0.954
Statistical characteristics	**Average =**		0.952
	STD =		0.00778
	CoV =		0.00817

Table 4. Sum of negative and positive flexural capacities of test specimens

Specimen	Negative flexural capacity (kN)	Positive flexural capacity (kN)	Sum of flexural capacities (kN)	Ratio of sum between T-section beam and CB-Rec/ CB-Rec-2
CB-Rec-2	320[(a)]	240[(a)]	560	100%
CB-T-2	500[(a)]	320[(a)]	820	146%
T-section beam with an FRP-strengthened web opening of 600 mm × 280 mm	256[(b)]	231[(c)]	487	87.0%
T-section beam with an FRP-strengthened web opening of 700 mm × 260 mm	265[(b)]	215[(c)]	480	85.7%
T-section beam with an FRP-strengthened web opening of 600 mm × 220 mm	380[(b)]	251[(c)]	631	113%
T-section beam with an FRP-strengthened web opening of 700 mm × 200 mm	388[(b)]	233[(c)]	621	111%

Note:

(a) Obtained from the FE analyses;

(b) Obtained from the tests;

(c) Obtained from the proposed strength model [35].

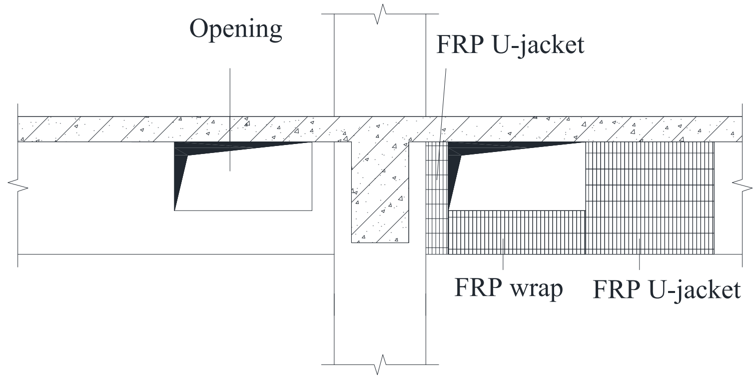

Figure 1. Beam opening (BO) technique

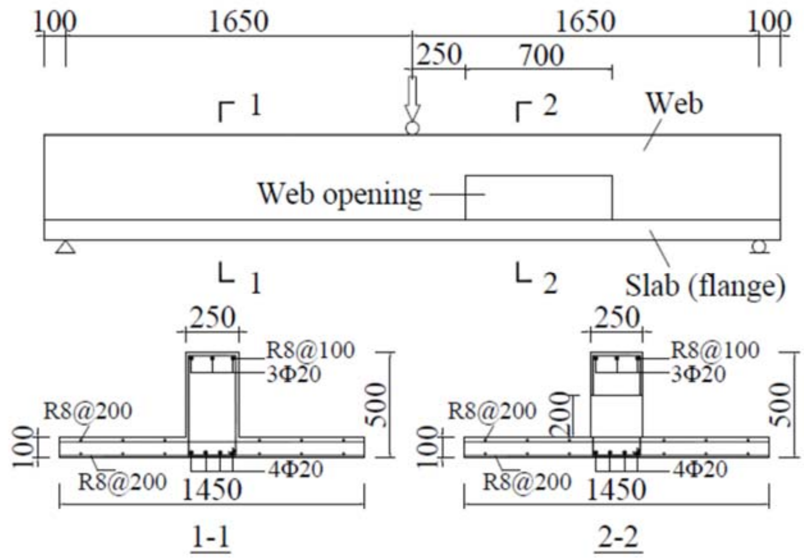

Note: R8-smmoth steel bars of 8 mm in diameter; Φ20-deformed steel bars of 20 mm in diameter.

Figure 2. Details of test specimen (O-700×200) (dimensions in mm)

Figure 3. Making a pre-formed opening in an RC T-section beam

 

(a) (b)

 

(c) (d)

Figure 4. Making a post-cut opening in an RC T-section beam

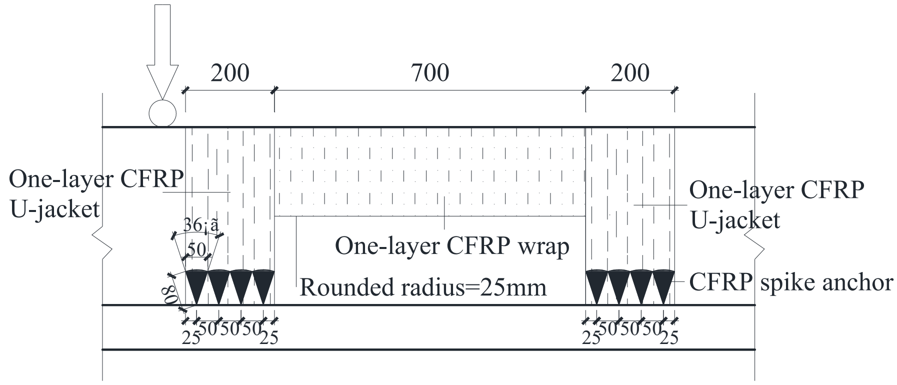

(a) CFRP strengthening region

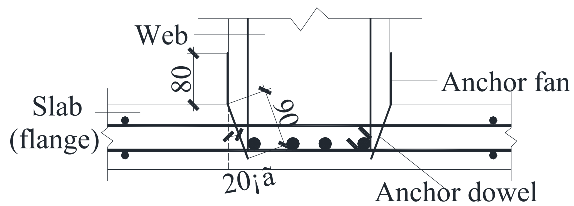

(b) CFRP spike anchors shown on the beam cross-section

(c) CFRP spike anchor

Figure 5. CFRP strengthening system (F-700×200) (dimensions in mm)


(a) (b)


(c) (d)

Figure 6. Installation of CFRP strengthening system

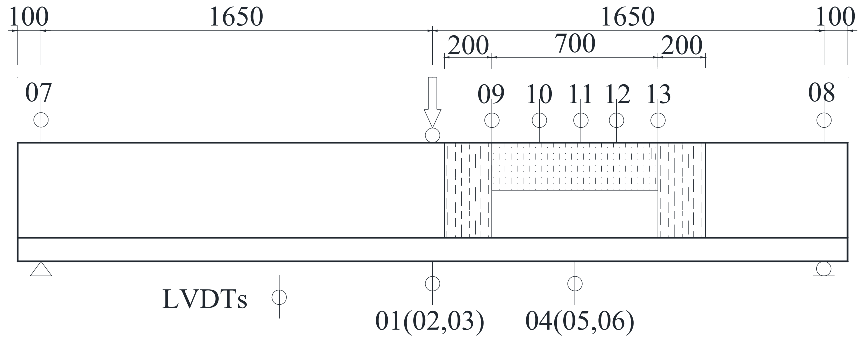

Figure 7. Layout of LVDTs (F-700×200) (dimensions in mm)

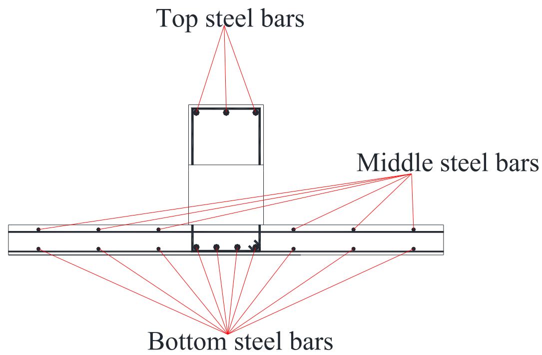

(a) Grouping of steel bars

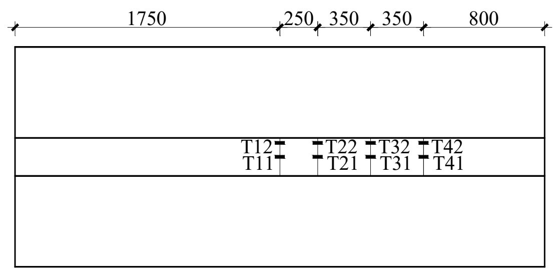

(b) Strain gauges on top steel bars

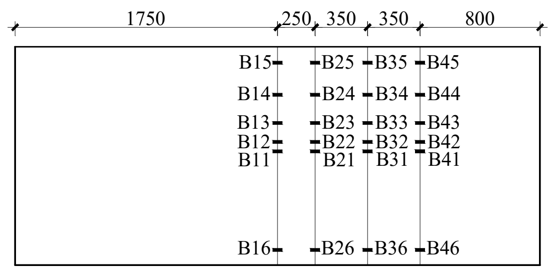

(c) Strain gauges on bottom steel bars

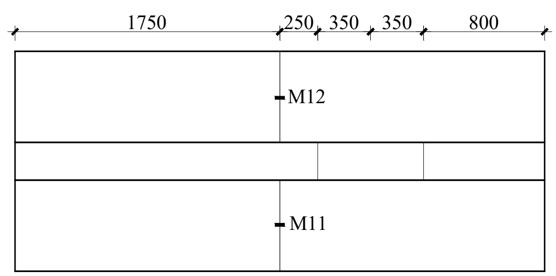

(d) Strain gauges on middle steel bars

Figure 8. Layout of strain gauges on steel bars (F-700×200) (dimensions in mm)

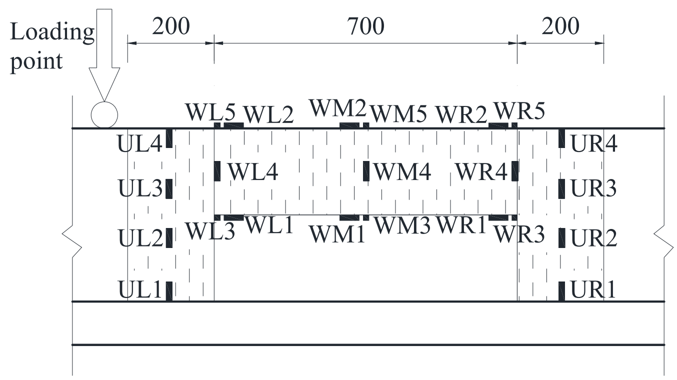

Note: L-left; M-middle; R-right; U-U-jacket; W-wrap; W*1/2 (*=L/M/R)-strain gauges in the longitudinal direction of the web chord, with 1 representing the strain gauge on the bottom surface of the web chord, and 2 representing the strain gauge on the top surface of the web chord; W*3/4/5 (*=L/M/R)-strain gauges in the hoop direction of the FRP wrap, with 3 representing the strain gauge on the bottom surface of the web chord, 4 representing the strain gauge on the side surface of the web chord, and 5 representing the strain gauge on the top surface of the web chord.

Figure 9. Layout of strain gauges on FRP (F-700×200) (dimensions in mm)

Figure 10. Test set-up

(a) O-600×220

(b) O-700×200

(c) F-600×220

(d) F-700×200

(e) F-600×280

(f) F-700×260

Figure 11. Failure modes of test specimens

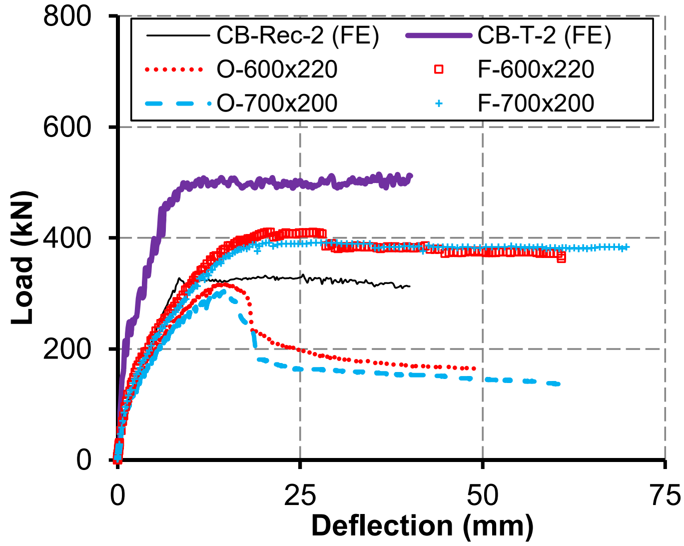

(a) Specimens with a small web opening

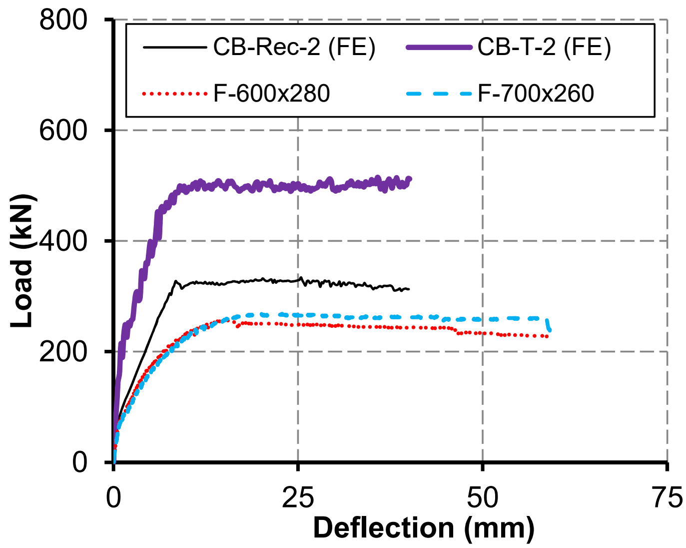

(b) Specimens with a medium web opening

Figure 12. Load-deflection curves of test specimens

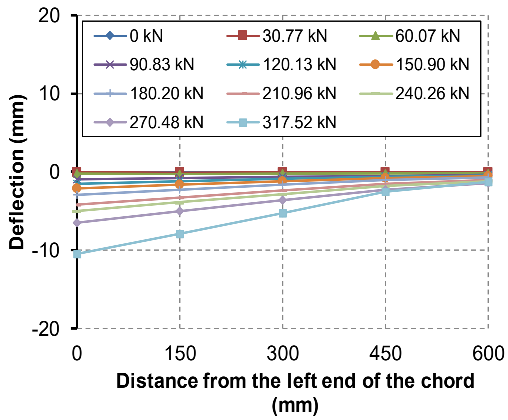

(a) O-600×220

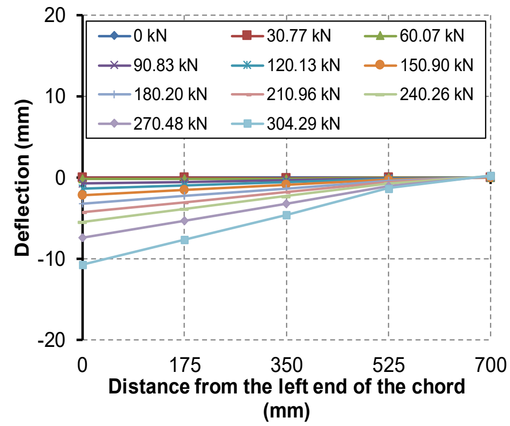

(b) O-700×200

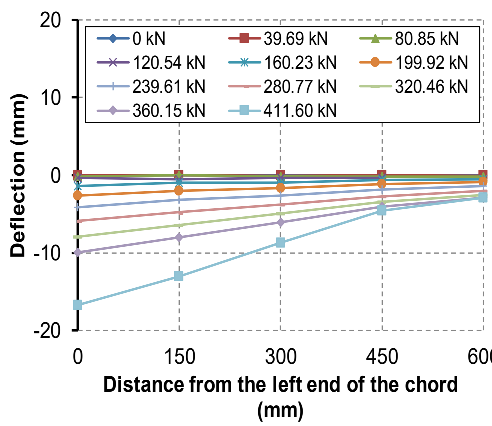

(c) F-600×220

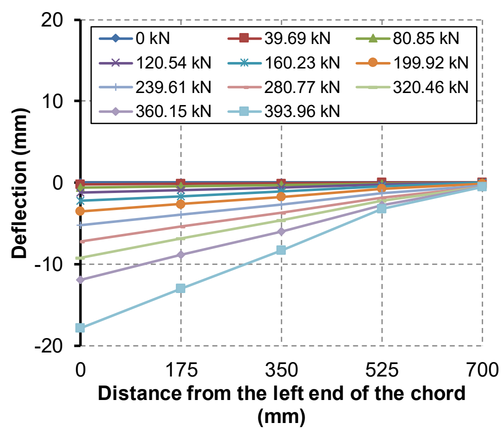

(d) F-700×200

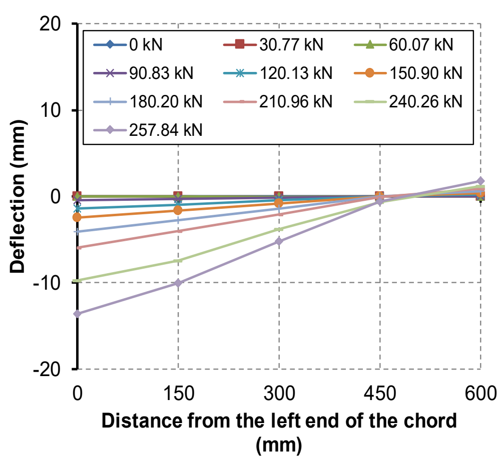

(e) F-600×280

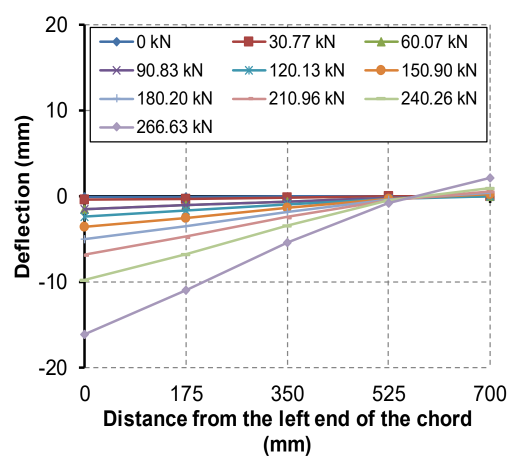

(f) F-700×260

Figure 13. Deflection of the web chord

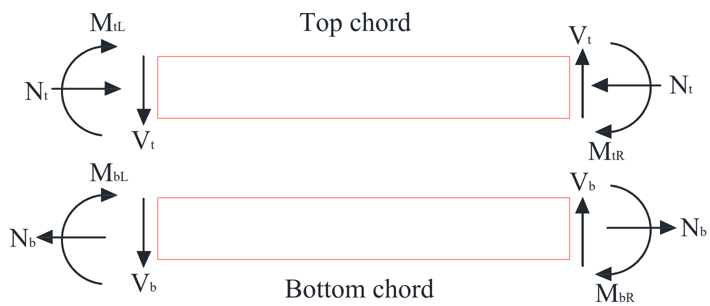

Figure 14. Free-body diagram of the chords

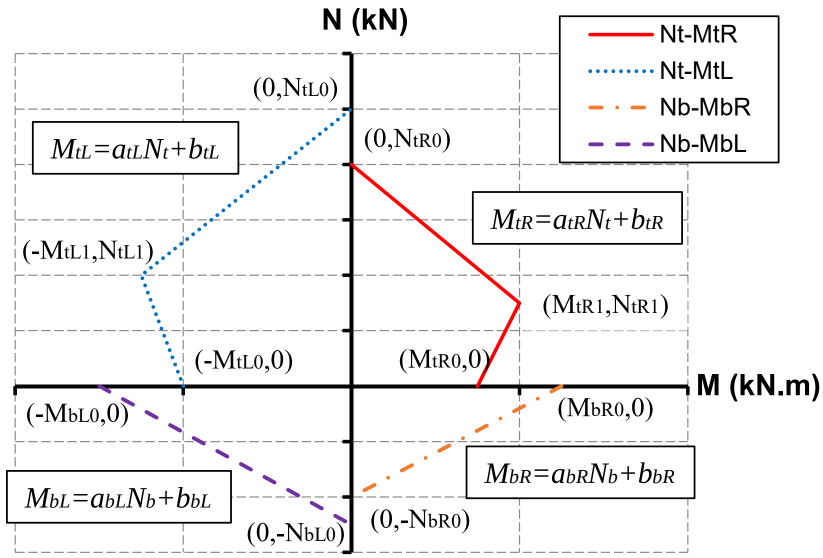

Figure 15. Simplified *N-M* curves of the chords